A Two-layer Framework for Mitigating the Congestion of Urban Power Grids Based on Flexible Topology with Dynamic Thermal Rating

Yi Su, *Graduated Student Member*, *IEEE*, Jiashen Teh, *Senior Member*, *IEEE*, Qian Luo, Kangmiao Tan, and Jiaying Yong

***Abstract*—The urban power grid (UPG) combines transmission and distribution networks. Past studies on UPG congestion mitigation have primarily focused on relieving local congestion while ignoring large-scale energy transfer with safety margins and load balancing. This situation is expected to worsen with the proliferation of renewable energy and electric vehicles. In this paper, a two-layer congestion mitigation framework is proposed, one which considers the congestion of the UPG with flexible topologies. In the upper-layer, the particle swarm optimization algorithm is employed to optimize the power supply distribution (PSD) of substation transformers. This is known as the upper-layer PSD. The lower-layer model recalculates the new PSD, known as the lower-layer PSD, based on the topology candidates. A candidate topology is at an optimum when the Euclidean distance mismatch between the upper- and lower-layer PSDs is the smallest. This optimum topology is tested by standard power flow to ascertain its feasibility. The optimum transitioning sequence between the initial and optimum topologies is also determined by the two-layer framework to minimize voltage deviation and line overloading of the UPG considering dynamic thermal rating. The proposed framework is tested on a 56-node test system. Results show that the proposed framework can significantly reduce congestion, maintain safety margins, and determine the optimum transitioning sequence.**

***Index Terms*—congestion mitigation, urban power grid, two-layer framework, transitioning sequence, dynamic thermal rating.**

I. Introduction

Urbanization has led to the formation of urban power grids (UPGs) which are hybrids of distribution and transmission networks [1]. With the increasing penetration of renewable distributed generation (RDG) and new loads [2], the congestion on the urban power grid [3] has become more pronounced, sudden and unpredictable, and needs to be addressed urgently. In addition, maintaining overall load balancing and safety margin is crucial for a UPG to accommodate the above uncertainties when relieving congestion. This has not been properly considered in previous studies. Also, the transition from the initial congestion state to the optimal state necessitates the collaboration of multiple devices.

Several methods have been proposed to relieve the congestion of UPGs. Generators are re-dispatched to reduce certain line loadings and network congestion by minimizing the cost of energy rescheduling in [4]. A day-ahead scheduling of generators and transmission switching is employed to enable transmission system operators (TSOs) to optimize network deployments in [5]. Although effective, these methods cannot be implemented in real-time. Hence, other methods with better real-time capability have been proposed. In [6], a real-time demand response (DR) program is deployed by retail electricity providers based on game theory. In addition, the interactions between load aggregators and distribution system operators (DSOs) are considered [7]–[8]. Nevertheless, all the above methods rely on load shedding to reduce congestion. This is undesirable because it leads to high load losses.

Other studies focus on the coordination between the TSO and DSO to achieve a holistic dispatching of network resources. A decentralized, secure, and economical generator dispatch plan of TSO and DSO on an hourly basis is proposed in [9], and it is further extended by considering the flexibility region construction and cooperation of TSO and DSO in optimal power flow dispatch in [10]. In [11], retailers are considered for hedging against network usage tariffs based on peak-load pricing of TSO and DSO. A bi-level optimization model across the transmission and distribution networks for coordinating the safety dispatch of large-scale distributed energy resources is proposed in [12]. Although the above methods can control the behavior of electricity consumption, load shedding during

Received: xx, xx, xxxx
Accepted: xx, xx, xxxx
Published Online: xx, xx, xxxx
Jiashen Teh (corresponding author) is with the School of Electrical and Electronic Engineering, Universiti Sains Malaysia (USM), Penang 11800, Malaysia (e-mail: jiashenteh@usm.my).
DOI: 10.23919/PCMP.2023.000139

peak hours is still unavoidable because of the lack of safety margin. In addition, they all ignore the potential of flexible networks in redirecting power flow to relieve congestion [13].

Flexible network topologies are optimized by the reinforcement learning algorithm [14] and particle swarm optimization algorithms (PSOA) [15]–[16] to improve the adequacy of power supply. Because these methods consider all circuit breakers (CBs) as switches when optimizing network topology, a large number of variables are involved in the optimization process. This prolongs simulation time. Several methods such as the Kruskal algorithm [17], a fast one-step method based on a set of binary descriptor matrices [18] and a heuristic based on a set of simplified load flow equations considering voltage and thermal limits [19] have been proposed to speed up simulations. However, the proposed methods have only been applied in the radial distribution network (DN), and this is different from the more complicated UPG structure. As a result, the simplification of objective functions and optimization constraints in a single framework shown by methods in [17]–[19] is not suitable for UPGs. Nonetheless, it is still clear that a flexible topology is beneficial for managing congestion.

In general, the literature review indicates the following shortcomings: 1) The congestion mitigation is mainly based on flexible load shedding, which does not meet the need for reliability of power supply; 2) UPG is a mixture of TSO and DSO with complex structure, so it is difficult to apply the flexible network reconfiguration directly as in the radial DN; and 3) The dynamic operation process from the congestion state to the optimal state is not considered. Thus, this paper solves the problem described above by proposing a two-layer congestion management framework for UPGs. The layering feature is due to the separation of the power supply distribution (PSD) of high-voltage substation transformers (STs) in the upper-layer from the flexible topology model in the lower-layer. The two-layer framework undergoes an optimization process whereby both models improve the solution of each other. This ensures that: 1) No new congestion is formed when existing congestion is cleared with the safety threshold, so load shedding can be avoided; 2) The computation of transmission and distribution network decoupling is suitable for large-scale UPGs; and 3) The optimum transitioning sequence between the initial and optimal states to minimize power system impacts based on dynamic thermal rating (DTR) is considered.

The main contributions of this paper are:

1) A two-layer congestion mitigation framework is proposed for UPGs. In the upper-layer model, PSOA is employed to optimize the PSD of STs, known as the upper-layer PSD. This represents the power supply from the transmission into the distribution networks. Searching the solution space at this level is faster because network topology is ignored and there is no need to perform power flow. The fittest upper-layer PSD is selected and passed down to the lower-layer model. In the lower-layer model, the optimal topology of the DN is determined. To speed up the searching process, all the load points are clustered into different unit groups and all the groups are considered in parallel. Each unit group has a set of optimum topology candidates and a PSD level is associated with every candidate. This is the lower-layer PSD. The candidate topology with the minimum distance between its associated lower-layer PSD and the upper-layer PSD is considered as the optimum topology of the unit group. The feasibility of the pair of optimum topology and lower-layer PSD is ascertained by the standard ACPF. This approach is more efficient and faster than one that considers the entire DN without forming unit groups.

2) The proposed framework has balanced power supply among STs in the upper-layer model to have the safety margin, so that it can tolerate more fluctuations of RDGs and EVs.

3) The proposed framework determines the optimum line switching sequence when optimizing the network topology based on DTR. Compared with the static thermal rating (STR) system, the DTR system systematically unlocks actual line capacity and the UPG can achieve rating gains at line switching.

The remainder of the paper is presented as follows. In Section II, the UPG model and the methods of forming unit groups and finding the optimum topology candidates are described. In Section III, the proposed two-layer congestion management framework is presented, while Section IV presents the optimum transitioning sequence model. Results and discussion are given in Section V, and the paper is concluded in Section VI.

II. Urban Power Grid Model

A. Modelling of UPG Components

Figure 1 shows the typical structure of the UPG and its characteristics are summarized in Table I (using Guangdong province, China as an example). As shown in Table I, each UPG comprises a smaller interconnected transmission network supplying multiple distribution networks, with multiple power sources within each UPS. This stands in contrast to the radial distribution network that relies on a single source. In terms of operator responsibilities, the transmission network operator primarily emphasizes regional advantages, such as optimizing generator economic dispatch. On the other hand, the UPG places a greater emphasis on power supply reliability, potentially achieving power flow optimization through a flexible topology.

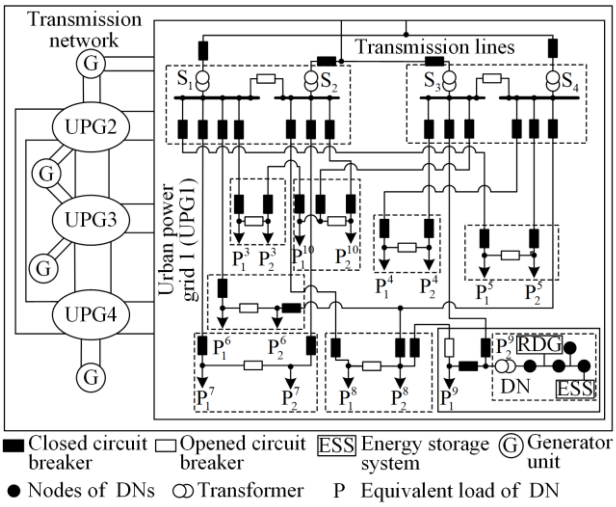

Fig. 1. A typical structure of an urban power grid.

TABLE I
COMPARING UPG, DISTRIBUTION AND TRANSMISSION NETWORKS IN GUANGDONG, CHINA

Network	Structural	Power (MVA)	Control object
UPG	Meshed network of a city	> 1000	Load & topology
Distribution network	Radial network of towns within a city	1–50 (one line)	Load
Transmission network	Meshed network of multiple cities	50–200 (one line)	Generators

As seen from Fig. 1, UPG1 has 45 CBs, resulting in 2^{45} candidate solutions to be considered. The large numbers of variables can be reduced by directly considering the lines themselves as the control variables. Thus the simplified topology of UPG1 can be obtained in Fig. 2, while considering that the STs are the power sources.

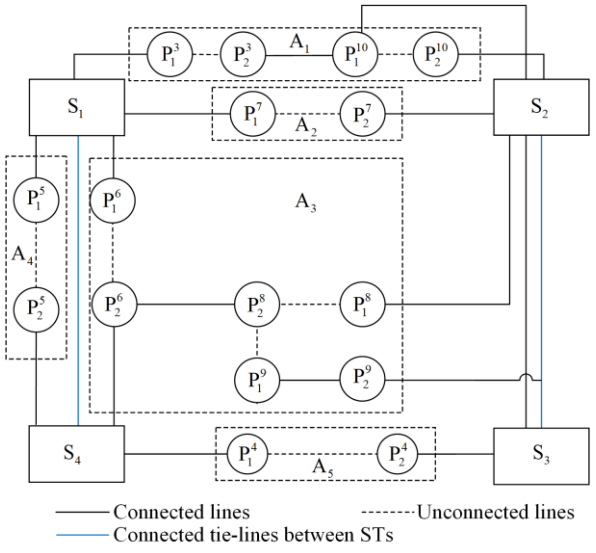

Fig. 2. Simplified topology of UGP1.

Figure 2 shows that this method needs to consider only the switching of 24 lines (2^{24} candidate solutions).

B. Unit Groups Formation Rules

The load point of the UPG is clustered into different unit groups to further speed up simulation. The general consideration when forming a particular unit group is that any two load points should be connected, either directly or indirectly, without passing through any STs. This method simplifies the topology optimization process because the network of each unit group is smaller and therefore can be handled more efficiently than optimizing the topology of the entire bigger DN without grouping. It also makes the UPG work as the radial topology to avoid the high-low voltage ring network. The step-by-step process of forming a unit group is as follows:

1) Randomly select a load as the initial member of the first unit group A_1. Then, identify all the other loads that are connected to the selected load without passing through any STs as the new members of A_1. For example, based on UPG1 in Fig. 1, the load P_2^3 is selected at random and initialized as the first member of A_1. Then, because P_2^3 is connected to P_1^3, P_2^{10} and P_1^{10} without passing through any ST, these additional load points are also included into group A_1. Hence, the final membership of A_1 is $\{P_1^3, P_2^3, P_1^{10}, P_2^{10}\}$.

2) The load points that have been identified within a group are excluded from all the subsequent considerations. The above process is repeated with a new load point until all the remaining load points have been assigned to a group. Using the same example, 5 unit groups with 6, 3, 9, 3 and 3 switchable lines respectively are formed in UPG1, as shown in Fig. 2. Thus, the candidate solutions are reduced to 2^6, 2^3, 2^9, 2^3 and 2^3 for A_1 to A_5, respectively. These can be optimized in parallel quickly.

C. Optimum Topology Candidates

The line switching of each unit group produces a set of c possible topologies $\mathbf{\Omega}_{A_i}$. All possible topologies of the set can be listed because the number of lines in each unit group is small. An element of $\mathbf{\Omega}_{A_i}$ is represented by the binary string variable $\psi_c^{A_i}$, i.e., $\psi_c^{A_i} \in \mathbf{\Omega}_{A_i}$, while each binary number represents a line status (close/open) of the unit group. For example, the unit group A_1 in Fig. 2 forms 64 combinations of line statuses ($c = 2^6 = 64$), and each combination, $\psi_c^{A_1}$ ($c \in [1,64]$), is a possible topology that A_1 can adopt. For example, the combination {0 0 0 0 0 0} represents that all the 6 lines are opened, and vice versa for the combination {1 1 1 1 1 1}.

Only the topologies that can form the radial DN are considered as the optimum topology candidates, notated by the variable $\psi_f^{A_i}$, i.e., $\psi_f^{A_i} \in \mathbf{\Omega}_{A_i}$. The radial network is advantageous because it avoids a closed loop current that is 1.34 times larger than the normal current [20]. Hence it also avoids overloading and cascading failures.

This approach is adopted by the China National Grid Company [21].

The optimum topology candidates are determined by examining the $\boldsymbol{B}_{\mathrm{LS}}(\psi_c^{\mathrm{A}_i})$ binary matrix. The binary values can indicate whether each load point is receiving power from only one ST in the candidate topology, which is the main characteristic of a radial network. A topology is radial when the summation of each row in the binary matrix is equal to one. For example, the topology {1 0 1 0 1 1} of the unit group A_1 in Fig. 2 has the following $\boldsymbol{B}_{\mathrm{LS}}(\psi_c^{\mathrm{A}_i})$ binary matrix, which means a radial network:

$$\boldsymbol{B}_{\mathrm{LS}}(1\,0\,1\,0\,1\,1)=\begin{array}{c} \\ \mathrm{P}_1^3 \\ \mathrm{P}_2^3 \\ \mathrm{P}_1^{10} \\ \mathrm{P}_2^{10} \end{array}\begin{array}{c} \begin{array}{ccc} \mathrm{S}_1 & \mathrm{S}_2 & \mathrm{S}_3 \end{array} \\ \begin{bmatrix} 1 & 0 & 0 \\ 0 & 0 & 1 \\ 0 & 0 & 1 \\ 0 & 1 & 0 \end{bmatrix} \end{array} \tag{1}$$

where $\mathrm{S}_1, \mathrm{S}_2, \mathrm{S}_3$ represent the substation transformer 1, 2, 3; while $\mathrm{P}_1^3, \mathrm{P}_2^3, \mathrm{P}_1^{10}, \mathrm{P}_2^{10}$ represent the loads in the distribution network A_1 as shown in Fig. 2.

III. Two-Layer Congestion Management Framework

A. Overview of the Proposed Framework

Considering the entire UPG when mitigating congestion creates a high-dimensionality problem that is difficult to solve. Consequently, a novel congestion management framework here is proposed, as shown in Fig. 3. The proposed framework operates on two layers: the upper layer which manages the power supplies of STs without any topological constraints, and the lower layer which identifies the appropriate topology for power supplies in each unit group. This framework involves an iterative interaction between the upper and lower layers to address the interdependent relationship between the power supplies of STs and the topology of unit groups.

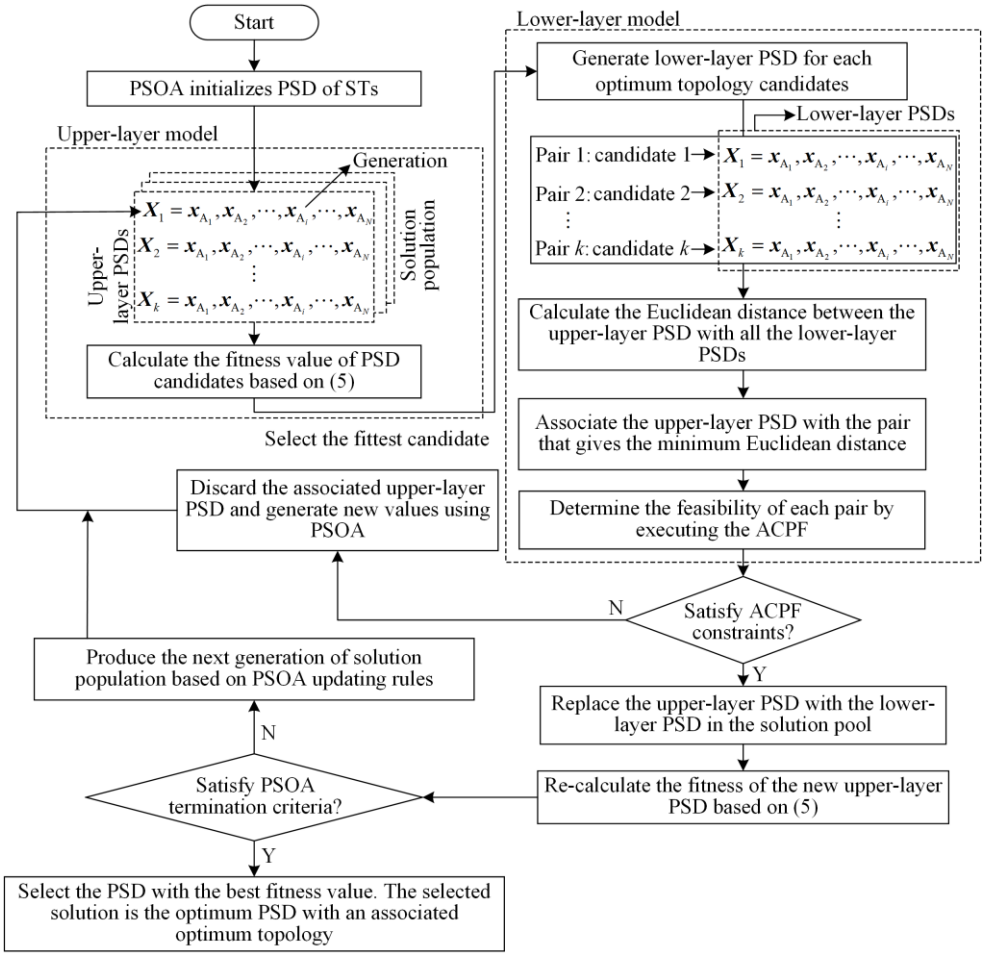

Fig. 3. Proposed two-layer congestion management framework.

The proposed framework begins with the PSOA initializing the first generation of solution population. Each solution is a set of normalized values which represent the PSD of STs. This first generation of solutions is applied to the upper-layer model, where their fitness values are calculated. The fittest solution is selected and passed down to the lower-layer model. The factors considered in the calculation are the optimal and aver-

age loading rates of STs and the tie-line capacities between the STs and DN. These factors ensure a balanced PSD and avoid the overloading of the tie-lines. The topology of the DN is not considered in the upper layer.

The lower-layer model determines its own set of PSD for each optimum topology candidate. The candidate topology that corresponds to the smallest Euclidean distance mismatch between the upper- and lower-layer PSDs is selected as the optimum topology. Therefore, the upper-layer PSD also corresponds to a pair of lower-layer PSD and optimum topology. The feasibility of the pair is determined with the power flow constraints. The power output is fixed to the value of the lower-layer PSD, since the lower-layer PSD is already the actual power output that should be injected into the DN during power flow analysis. Considering the power output as dispatchable during this time may produce a different final power output.

If the pair of lower-layer PSD and optimum topology cannot satisfy the power flow constraints, the corresponding upper-layer PSD is discarded and replaced with a new solution generated by the PSOA, while the new upper-layer PSD goes through the upper- and lower-layer models again. On the other hand, if the power flow constraints are satisfied, the lower-layer PSD will replace the corresponding upper-layer PSD in the existing solution population. The new fitness value of the updated upper-layer PSD is then calculated and stored.

At the end of each cycle, the next generation of solution is produced based on the PSOA rule and the two-layer process is repeated. The PSOA stops when the difference of the best fitness values between two generations is less that 10^{-3}. The candidate solution, which is the set of PSDs with the best fitness value in the final generation is selected as the ultimate solution. The PSD is also associated with an optimum topology of the distribution network. The details of the proposed framework are described next.

B. Initialization

The PSOA initializes a population of PSD levels of all the STs, which serve as the power supply of *N* unit groups in the DN, as follows:

$$\boldsymbol{X}_k = \left[\boldsymbol{x}_{\mathrm{A}_1}, \boldsymbol{x}_{\mathrm{A}_2}, \cdots, \boldsymbol{x}_{\mathrm{A}_i}, \cdots, \boldsymbol{x}_{\mathrm{A}_N} \right] \tag{2}$$

$$\boldsymbol{x}_{\mathrm{A}_i} = [\boldsymbol{x}_{\mathrm{S}_1}^{\mathrm{A}_i,\mathrm{up}}, \boldsymbol{x}_{\mathrm{S}_2}^{\mathrm{A}_i,\mathrm{up}}, \boldsymbol{x}_{\mathrm{S}_j}^{\mathrm{A}_i,\mathrm{up}}, \cdots, \boldsymbol{x}_{\mathrm{S}_{\mathrm{m}_i}}^{\mathrm{A}_i,\mathrm{up}}] \tag{3}$$

where $\boldsymbol{X}_k$ represents the *k*th solution population determined by the PSOA in each generation and *k* is the number of particles produced in each generation by the PSOA; $\boldsymbol{x}_{\mathrm{A}_i}$ represents the matrix of power supply level of A_i; while $x_{\mathrm{S}_j}^{\mathrm{A}_i,\mathrm{up}}$ is the normalized power supply of S_j to A_i in the upper layer, and its value is between 0 and 1, representing a ratio of the total power capacity of the ST.

For example, in Fig. 2, one of the variables $\boldsymbol{X}_k$ is shown as (4), which is a 13-dimension variable, as compared to a 24-dimension variable (24 lines) if the topology of the DN is optimized without using the proposed two-layer approach.

$$\boldsymbol{X}_k = \begin{bmatrix} x_{\mathrm{S}_1}^{\mathrm{A}_1,\mathrm{up}}, x_{\mathrm{S}_2}^{\mathrm{A}_1,\mathrm{up}}, x_{\mathrm{S}_3}^{\mathrm{A}_1,\mathrm{up}}, x_{\mathrm{S}_1}^{\mathrm{A}_2,\mathrm{up}}, x_{\mathrm{S}_2}^{\mathrm{A}_2,\mathrm{up}} \\ x_{\mathrm{S}_1}^{\mathrm{A}_3,\mathrm{up}}, x_{\mathrm{S}_2}^{\mathrm{A}_3,\mathrm{up}}, x_{\mathrm{S}_3}^{\mathrm{A}_3,\mathrm{up}}, x_{\mathrm{S}_4}^{\mathrm{A}_3,\mathrm{up}}, x_{\mathrm{S}_1}^{\mathrm{A}_4,\mathrm{up}}, x_{\mathrm{S}_4}^{\mathrm{A}_4,\mathrm{up}} \\ x_{\mathrm{S}_3}^{\mathrm{A}_5,\mathrm{up}}, x_{\mathrm{S}_4}^{\mathrm{A}_5,\mathrm{up}} \end{bmatrix} \tag{4}$$

Please note that the random initialization of PSO might influence the final performance, but it can be solved by improvement of PSOA, which is not the key in this paper. Other PSOA parameters are employed from [16].

C. *Upper-layer Model*

The upper layer model minimizes the following fitness function that is comprised of three objective functions:

$$F_{\mathrm{up}} = \min(\mu_1 F_1 + \mu_2 F_2 + \mu_3 F_3) \tag{5}$$

where F_1 is the first objective function that shows the deviation between the upper-layer PSDs given by the PSOA and the optimal loading rate of STs; F_2 is the second objective function and is similar to F_1, but shows the deviation with the average loading rate of the ST instead; F_3 is the third objective function that indicates whether the ratings of all the lines between different STs can support the upper-layer PSD to avoid overloading; the variables μ_1, μ_2 and μ_3 are the weights that indicate the emphasis levels of the objective functions, which are set based on user requirement. In this paper, they are set to 1, 10, and 100, respectively.

Note that the PSD and loading rate of STs are the same because the power supply is delivered to the DN through the STs. Loading the STs at the optimal rate, ξ^{ref} minimizes transformer losses while meeting power demand [22]. This is considered in F_1 to ensure optimum PSDs of the STs. F_1 is determined as:

$$F_1 = \left(\sum_{j=1}^{M} \left| \xi_j - \xi_j^{\mathrm{ref}} \right| \right) / M \tag{6}$$

$$\xi_j = \left(\sum_{i=1}^{N} x_{\mathrm{S}_j}^{\mathrm{A}_i,\mathrm{up}} \times C(\mathrm{A}_i) \right) / C_j \tag{7}$$

where ξ_j, ξ_j^{ref} represent the actual and optimal loading rates of the *j*th ST; *M* is the number of STs connected with load demand; *N* is the number of unit groups in the UPG; $C(\mathrm{A}_i)$ is the power demand of the unit group A_i; and C_j is the rated capacity of the *j*th ST.

F_2, the additional factor, is considered because it is not possible to always load STs optimally. Therefore, F_2 is determined to ensure a margin of safety, i.e.:

$$F_2 = \left(\sum_{j=1}^{M} \left| \xi_j - \overline{\xi_j} \right| \right) / M \tag{8}$$

$$\overline{\xi_j} = \left(\sum_{j=1}^{M} \xi_j\right)/M \tag{9}$$

where $\overline{\xi_j}$ is the average loading rate of the *j*th ST.

F_3 is performed by comparing the tie-line ratings with the PSD of the STs, which shows the amount of power to be injected into the DN, i.e.:

$$F_3 = \sum_{i=1}^{N} \sum_{j=1}^{m_i} f_{l_1,\text{up}}^{\text{A}_i} \tag{10}$$

$$f_{l_1,\text{up}}^{\text{A}_i} = \begin{cases} 1, x_{\text{S}_j}^{\text{A}_i,\text{up}} C(\text{A}_i) \geqslant C_{l_1}^{\max} \\ 0, x_{\text{S}_j}^{\text{A}_i,\text{up}} C(\text{A}_i) < C_{l_1}^{\max} \end{cases}, \forall l_1 \tag{11}$$

where $f_{l_1,\text{up}}^{\text{A}_i}$ is the value indicating whether line l_1 is overload; and $C_{l_1}^{\max}$ is the maximum capacity of line l_1.

D. Lower-layer Model

The lower-layer model determines the optimum topology by minimizing the following function:

$$F_{\text{low}} = \min(\mu_4 F_4^{\text{A}_i} + \mu_5 F_5^{\text{A}_i}) \tag{12}$$

where the variables μ_4 and μ_5 are the weights of $F_4^{\text{A}_i}$ and $F_5^{\text{A}_i}$ that indicate the emphasis levels of the objective functions, they are set based on user requirement and in this paper, they are set to 10 and 1, respectively; $F_4^{\text{A}_i}$ is the first objective function that ensures that the chosen topology of A_i is optimum for minimizing the Euclidean distance mismatch between the upper- and lower-layer PSD, i.e.:

$$F_4^{\text{A}_i} = \sqrt{\sum_{j=1}^{m_i} \left[x_{\text{S}_j}^{\text{A}_i,\text{up}} - x_{\text{S}_j}^{\text{A}_i,\text{low}}(\psi_f^{\text{A}_i}) \right]^2} \tag{13}$$

such that,

$$\sum_{j=1}^{m_i} x_{\text{S}_j}^{\text{A}_i,\text{up}} = 1 \tag{14}$$

$$x_{\text{S}_j}^{\text{A}_i,\text{low}}(\psi_f^{\text{A}_i}) = C_{\text{S}_j}^{\text{A}_i}(\psi_f^{\text{A}_i})/C(\text{A}_i) \tag{15}$$

where $x_{\text{S}_j}^{\text{A}_i,\text{low}}$ is the lower-layer PSD that is determined based on the optimum topology candidate; and $C_{\text{S}_j}^{\text{A}_i}(\psi_f^{\text{A}_i})$ is the real power demand of A_i from S_j based on the topology $\psi_f^{\text{A}_i}$. For example, $\psi_f^{\text{A}_i}$ is based on the same example in Fig. 2 and the unit group A_i, while $F_4^{\text{A}_i}$ is further elucidated as shown in Table II. For the purpose of this example, it is assumed that the upper-layer PSDs of A_i are $x_{\text{S}_1}^{\text{A}_1,\text{up}} = 0.2$, $x_{\text{S}_2}^{\text{A}_1,\text{up}} = 0.3$ and $x_{\text{S}_3}^{\text{A}_1,\text{up}} = 0.5$, with all load points in A_i equal.

Table II shows the resultant $F_4^{\text{A}_i}$ values of all the optimum topology candidates. As seen, the topology {1 0 1 0 1 1} has the minimum $F_4^{\text{A}_i}$ value of 0.07 and therefore it is chosen as the optimum topology. Calculating Table II is fast because the list of all the optimum topology candidates can be determined comprehensively. It is apparent from this example that the choice of the optimum topology depends on the upper-layer PSD that is determined by the PSOA.

TABLE II

EXAMPLE THAT ELUCIDATES THE CALCULATION OF VARIABLE $F_4^{\text{A}_i}$

$\psi_f^{\text{A}_i}$	$x_{\text{S}_1}^{\text{A}_1,\text{low}}$	$x_{\text{S}_2}^{\text{A}_1,\text{low}}$	$x_{\text{S}_3}^{\text{A}_1,\text{low}}$	$F_4^{\text{A}_i}$
011011	0	$\frac{C(\text{P}_2^{10})}{C(\text{A}_1)} = 0.25$	$\frac{\left[C(\text{P}_1^3)+C(\text{P}_2^3)+C(\text{P}_1^{10})\right]}{C(\text{A}_1)} = 0.75$	0.32
011110	0	1	0	0.88
011101	0	0	1	0.62
101110	0.25	0.75	0	0.67
101011	0.25	0.25	0.5	**0.07**
101101	0.25	0	0.75	0.39
110110	0.50	0.5	0	0.62
110011	0.50	0.25	0.25	0.39
110101	0.50	0	0.5	0.42
111010	0.75	0.25	0	0.74
111100	1	0	0	0.99

To distinguish $F_4^{\text{A}_i}$ with similar values, $F_5^{\text{A}_i}$ is determined. This indicates whether the tie-line ratings between the STs and DN can support the lower-layer PSD, i.e.:

$$F_5^{\text{A}_i} = \sum_{j=1}^{m_i} f_{l_2,\text{low}}^{\text{A}_i} \tag{16}$$

such that,

$$f_{l_2,\text{low}}^{\text{A}_i} = \begin{cases} 1, x_{\text{S}_j}^{\text{A}_i,\text{low}}(\psi_f^{\text{A}_i}) \times C(\text{A}_i) \geqslant C_{l_2}^{\max} \\ 0, x_{\text{S}_j}^{\text{A}_i,\text{low}}(\psi_f^{\text{A}_i}) \times C(\text{A}_i) < C_{l_2}^{\max} \end{cases}, \forall l_2 \tag{17}$$

where $x_{\text{S}_j}^{\text{A}_i,\text{low}}(\psi_f^{\text{A}_i})$ represents the normalized power supply of S_j to A_i in the lower layer; the value of $f_{l_2,\text{low}}^{\text{A}_i}$ shows whether line l_2 is overload; $C_{l_2}^{\max}$ is the maximum capacity of line l_2.

It is important to mention again that the lower-layer model is applied on every unit group in parallel. Therefore, equations (12)–(17) are performed at the same time on all unit groups.

At this point, a pair of variables are associated with each unit group: 1) lower-layer PSD; and 2) the optimum topology. However, it has not been determined whether employing the pair can satisfy all the conventional AC power flow (ACPF) constraints and therefore, whether or not it is feasible. The lower-layer PSD is used as fixed, instead of dispatchable, power supply of the ACPF to ensure that the power output is the same as the lower-layer PSD levels. The ACPF is given as:

$$p_a = u_a \sum_{b=1}^{n} u_b (G_{ab}\cos\phi_{ab} + B_{ab}\sin\phi_{ab}) \tag{18}$$

$$q_a = u_a \sum_{b=1}^{n} u_b (G_{ab}\sin\phi_{ab} - B_{ab}\cos\phi_{ab}) \tag{19}$$

$$u_a^{\min} \leqslant u_a \leqslant u_a^{\max}, \forall a \tag{20}$$

$$p_{\text{S}_j} \leqslant p_{\text{S}_j}^{\max}, \forall \text{S}_j \tag{21}$$

$$I_l \leqslant I_{\max,l}, \forall l \tag{22}$$

where a and b are the indices of from- and to- nodes in the UPG; u_a and u_b is the voltage of node a and b; $u_a^{\min}$ and $u_a^{\max}$ is the minimum and maximum voltage of node a; p_a and q_a are the active and reactive power of node a; G_{ab} and B_{ab} are the conductance and susceptance of the line between nodes a and b; p_{S_j} and $p_{S_j}^{\max}$ are the power supply and maximum capacity of the jth ST; while I_l and $I_{\max,l}$ are the actual and maximum current ratings of line l.

$I_{\max,l}$ can either be the static thermal rating (STR) or the dynamic thermal rating (DTR). The STR is calculated based on a fixed set of conservative weather assumptions and the DTR is calculated based on real-time weather conditions as:

$$I_{\mathrm{DTR}} = \sqrt{\frac{Q_{\mathrm{c}}(T_{\mathrm{a}}, T_{\mathrm{c}}, V_{\omega}, \theta_{\omega}) + Q_{\mathrm{r}}(T_{\mathrm{a}}, T_{\mathrm{c}}) - Q_{\mathrm{s}}}{R(T_{\mathrm{c}})}} \quad (23)$$

where $V_{\omega}, \theta_{\omega}$ are the wind speed and angle; $T_{\mathrm{a}}, T_{\mathrm{c}}$ are the ambient and conductor temperature; Q_{c}, Q_{r} and Q_{s} are the convection heat loss, radiated heat loss and heat gain; and $R(T_{\mathrm{c}})$ is the resistance of conductor at temperature T_{c}.

Equation (23) is the steady state DTR calculation described in [23]. The equation shows that the current capacity of lines is greatly affected by micro meteorological conditions.

If the power flow is not feasible, which happens when the ACPF constraints cannot be satisfied and convergence cannot be achieved, the upper-layer PSD associated with the pair of variables is discarded and a new upper-layer PSD is generated by the PSOA. On the other hand, if the power flow is feasible, then the lower-layer PSD will replace the upper-layer PSD in the candidate solution pool and the fitness value in (5) is recalculated. This process is repeated on all the solution population.

IV. State Transition Sequence Model

In Section III, both the optimum PSD and the optimum topology of the DN are obtained. Although the optimized state of the UPG can be found, the sequence of transitioning between the initial to the final states is unknown and has never been considered. This is an important factor that this section intends to address because the transitioning sequence determines whether certain power system conditions can be met during the transitioning and before the optimized state is reached. The conditions that are considered here are: 1) line overloading; and 2) overvoltage of nodes.

For example, consider that the initial and final states of A_i are {**0 1** 1 **1** 1 **0**} and {**1 0** 1 **0** 1 **1**}, respectively. From the initial to the final states, four lines have been switched, i.e., the second $(P_1^3 - P_2^3)$ and fourth $(P_1^{10} - P_2^{10})$ lines are switched off, while the first $(S_1 - P_1^3)$ and sixth $(P_1^{10} - S_3)$ lines are switched on. However, the sequence of line switching and the effect of a particular switching towards the power system conditions are unknown. The state transitioning sequence model is thus presented next.

Considering that the transition from the initial to the final optimal states requires Z switchings, the multi-objective of the state transitioning sequence model is given as:

$$\Theta = \min \sum_{R=1}^{Z} \left[\frac{\tau_1}{H} \left(\sum_{a=1}^{H} f_{\mathrm{U}}^R(a) \right) + \frac{\tau_2}{L} \left(\sum_{l=1}^{L} f_{\mathrm{I}}^R(l) \right) \right] \quad (24)$$

where H and L are the numbers of the nodes and lines, respectively; while R represents the index of the switching actions; $f_{\mathrm{U}}^R(a)$ and $f_{\mathrm{I}}^R(l)$ are the first and second objective functions; the variables τ_1 and τ_2 are the weights that indicate the emphasis levels of the objective functions, which are set based on the priority of the user, and their values can be set as equal if both conditions are equally important.

$f_{\mathrm{U}}^R(a)$ is the index of nodal voltage deviation from the ideal rated voltage (1 p.u.), i.e.:

$$f_{\mathrm{U}}^R(a) = \begin{cases} \dfrac{\left| u_a^R - 1 \right|}{0.07}, & 0.93 \leqslant u_a^R \leqslant 1.07 \\ 1, \text{ others} \end{cases} \quad (25)$$

where u_a^R represents the voltage (p.u.) of node a after the Rth transition. Note that the voltage is considered not feasible if it deviates 7% from the rated value [24].

$f_{\mathrm{I}}^R(l)$ is the index of line loading deviation from the maximum ratings of the line, i.e.:

$$f_{\mathrm{I}}^R(l) = \begin{cases} \dfrac{I_l^R}{I_{\max,l}}, I_l^R \leqslant I_{\max,l} \\ 1, I_l^R > I_{\max,l} \end{cases} \quad (26)$$

where I_l^R is the actual current of line l after the Rth transition, and $I_{\max,l}$ is the maximum line rating, which can either be STR or DTR.

Based on the same A_1 example mentioned earlier, there are 24 (4×3×2×1) different transitioning sequences between the initial and final states because 4 lines are switched. In each sequence, the states of the 4 lines are changed one at a time. Based on (24), the sequence with the biggest Θ value is the most undesirable because it has the total worst impact on the power system conditions. On the other hand, the sequence with the smallest Θ value is the most desirable and is the optimum transitioning sequence between the initial and final states.

The number of possible transitioning sequences is reduced based on the following rules: 1) the switching operation gives priority to closing over opening lines to

ensure adequate power supply; and 2) the closing and opening of lines should be executed in pairs to ensure a radial network, and to avoid closed loop flow. With these two rules, the number of transitioning sequences of A_1 is reduced from 24 to 4.

V. Results And Discussions

The test system used in this study is a 56-node UPG, as shown in Fig. 4.

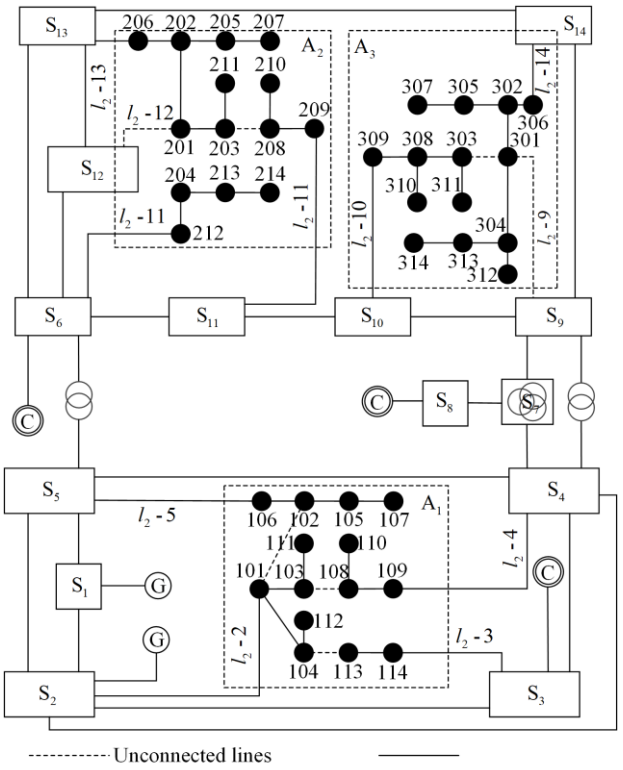

Fig. 4. The 56-node test system.

The test system is formed by combining one IEEE 14-node transmission network [25] and three IEEE 14-node distribution networks [26], with the latter used to describe the topology of the load points. The unit groups A_1, A_2 and A_3 in Fig. 4 are formed based on Section II. C. The total load demand of the UPG is 258.3 MVA and is obtained by increasing the original load level of each unit group by three times so that the total supply and demand levels are balanced. The rated capacity and optimal loading rate (ξ^{ref}) of all the STs in the test system are 75 kVA and 0.5, respectively. All the tie-lines between the STs and load points are considered to be the 110 kV 110-LGJ-95 lines from China with 60 MVA capacity. The per unit resistance and reactance of the lines are 0.035 and 0.13, respectively. The entire test system is considered to be in the same weather area to simplify DTR calculations in one of the case studies (case 4). All standard PSOA parameters [17] are used in the simulation, which is performed on a PC with AMD 5-3500U 2.10 GHz CPU and 8.00 GB of RAM. Note that the topology shown in Fig. 4 is the considered the initial state of the network. Four case studies are simulated and are described next.

Case 1, Load point multiplication, simulates the scenario of high load growth at several load points. These are spread across the entire UPG. STR is implemented in Case 1. The load points 104, 109, 203, 207 and 303 from different unit groups are selected at random and their load levels are doubled to create network congestion. This is mitigated by the proposed two-layer framework. The changes in the loading percentage of the tie-lines (between STs and unit groups) before and after congestion mitigation are shown in Fig. 5. The modifications of the network topology to enable the congestion mitigation are shown in Fig. 6.

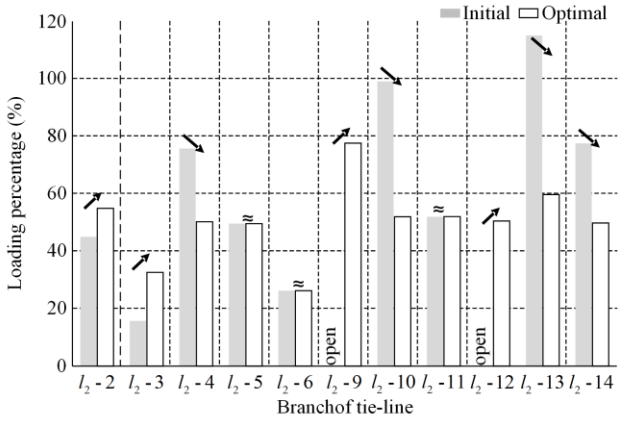

Fig. 5. Changes of loading percentage of the tie-lines in Case 1.

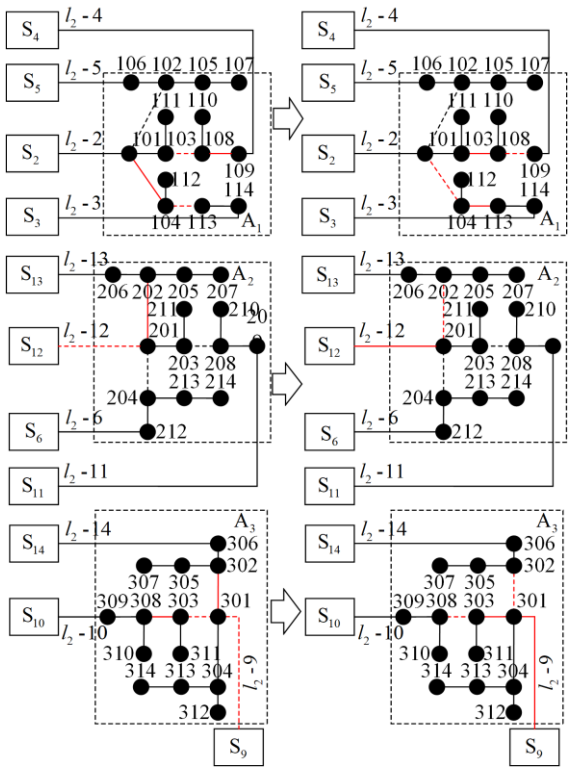

Fig. 6. Changes of topology for mitigating congestion in Case 1.

Figure 5 shows that the loading percentages among l_2-2, l_2-3 and l_2-4 that are connected with A_1 are more balanced after the congestion is relieved. The loading on l_2-4 is reduced by 25.5% and is transferred to l_2-2 and l_2-3, with their loadings increased by 9.9% and 16.9%, respectively. These changes are due to the two sets of load transfer as shown in Fig. 6, i.e.: 1) load points 108 and 110 are transferred from l_2-4 to l_2-2; and 2) load points 104 and 112 are transferred from l_2-2 to l_2-3. Figure 5 also shows that the overloading in l_2-13 connected with A_2 is relieved after employing the proposed framework. The loading of the tie-line is reduced by 55.4% because of the transfer of its load points 201, 203 and 211 to l_2-12, which is initially disconnected from A_2, as demonstrated in Fig. 6. Another overloaded tie-line l_2-10 connected with A_3 has also been relieved. Its loading is reduced by 47.1% by transferring its load points 303 and 311 to l_2-9, which is initially disconnected from A_3. Additionally, the load point 301 that is initially served by l_2-14 has also been transferred to l_2-9. This preempts the overloading of l_2-14 that already has an initial loading of 80%. The loading percentages of the remaining tie-lines (l_2-5, l_2-6 and l_2-11) are largely unchanged.

The effect of load increment on nodal voltage is also investigated and the results are shown in Fig. 7. It shows the voltage levels of every node before and after employing the proposed network congestion mitigation framework. Initially, the voltages of the nodes that are highlighted dip below the minimum acceptable level of 0.93 p.u. because of the significant increment of load demand. However, the transfer of load performed by the proposed framework as shown in Fig. 6 helps to improve the voltage levels back to within the acceptable range (0.93–1.07 p.u.).

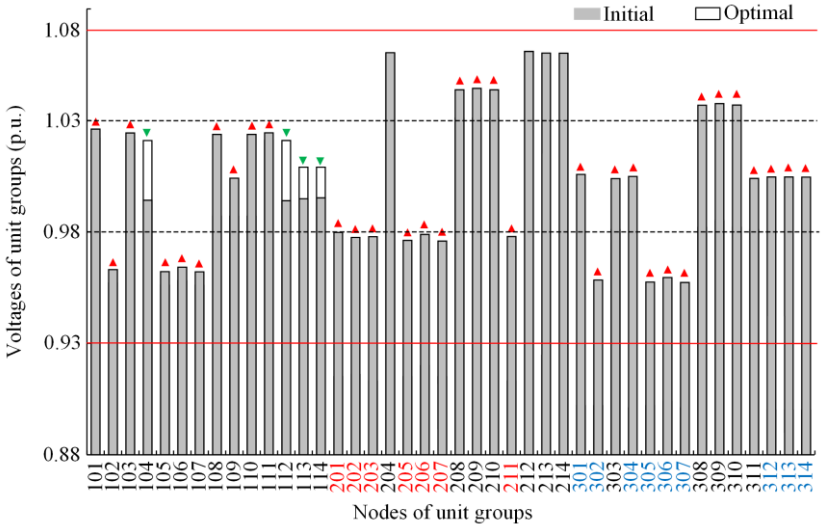

Fig. 7. Changes of voltage for mitigating congestions in Case 1.

Ultimately, all the results presented above show that the proposed framework can mitigate network congestion, with line overloading avoided and all nodal voltages maintained within the acceptable range.

Case 2, regional load growth, simulates large-scale demand growth by increasing the entire load demand of the unit groups A_2 and A_3 by 30% and 20%, respectively. STR is implemented, while the resultant congestion of the network is mitigated by employing the proposed framework which determines the optimum PSD and topology. All the corresponding line switching decisions of the optimum topology are shown in Table III. As large demand growth may cause overloading of STs, the loading conditions of STs are investigated and shown in Fig. 8. As seen, the optimal network topology enables all STs to be operated within their acceptable loading range [22] (40%–60%). The loading rates of S_2 and S_3 are initially less than 40%, but are improved to 42.5% and 41.4%, respectively, after the congestion on the network is cleared. This is possible because the tie-lines that are connected to the two STs have more available capacity now to serve more load points. At the same time, the initially overloaded S_{10}, S_{13} and S_{14} are relieved by 49.6%, 52.4% and 48.3%, respectively, and are all operating within the acceptable range after topology optimization. The reason is that more power supply can be drawn from other STs that are previously underutilized after the congestion is cleared. Subsequently, it reduces the power supply dependency of the three STs. As a result, the less overloaded STs are better prepared for supporting other STs during unexpected outages, and hence, have a better margin of operational risk.

TABLE III
CHANGES OF TOPOLOGY FOR MITIGATING CONGESTIONS IN CASE 2

Unit group	From node	To node	Initial	Optimized
A_1	S_3	114	1	0
	104	113	0	1
A_2	S_6	212	1	0
	S_{12}	201	0	1
	201	202	1	0
	201	204	0	1
A_3	S_9	301	0	1
	301	302	1	0
	303	308	1	0
	301	303	0	1

1 indicates connect; 0 indicates disconnect.

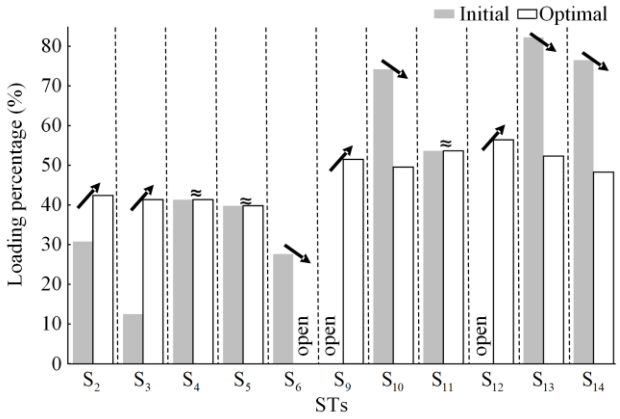

Fig. 8. Changes of loading percentages of STs in Case 2.

The voltage profiles of the STs before and after optimizing the network topology are shown in Fig. 9. It can be seen that the voltage of S_{14} has been improved from 0.927 p.u. to 0.97 p.u. after congestion mitigation. This is then within the acceptable operating voltage range of the STs (0.95–1.05 p.u.).

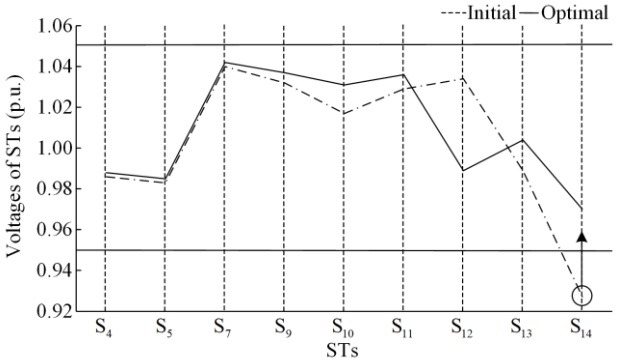

Fig. 9. Changes of nodal voltages of the STs in Case 2.

Case 3, line outage, simulates N-1 line outages with STR implemented. It is considered that tie-line l_2 - 2 of the test system has an outage. This outage cuts off power supply to load points 101, 103, 104, 111 and 112 and the subsequent priority is to restore all their power supplies. This can be achieved by closing one of the following three distribution lines: 103–108, 101–102 or 104–113. Each of these options can cause new congestion in other parts of the network and these need to be determined. If there is new congestion, it can be mitigated by the proposed framework.

For example, if we consider that the distribution line 103–108 is closed, the effect of this decision towards the loading of all the tie-lines between the STs and DN is shown in Fig. 10.

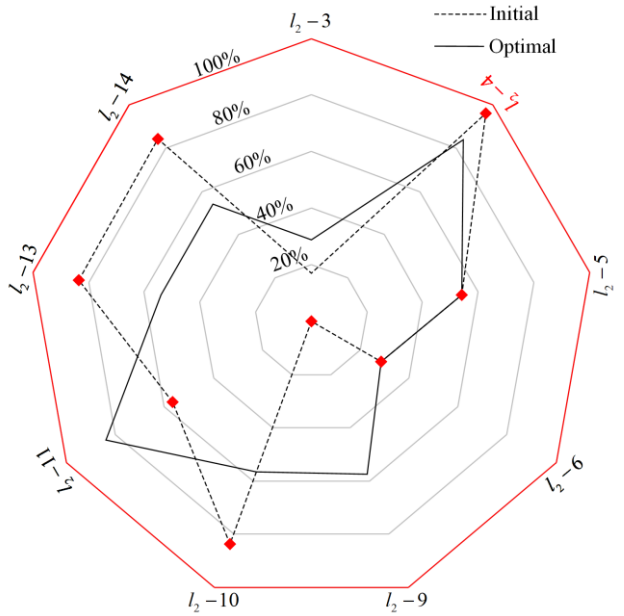

Fig. 10. Change of loading percentages of tie-lines in Case 3.

It can be seen that, although the decision restores the power supplies of the affected load points, tie-line l_2 - 4 is loaded to 95.9% of its maximum capacity. Essentially, it is no longer safe to further deploy the tie-line because the low margin of the remaining line capacity is very much at risk of overloading. In other words, tie-line l_2 - 4 is congested and this inhibits load growth of the unit group A_1. To overcome the congestion, the proposed framework is deployed. Figure 10 shows that the proposed framework is able to reduce the loading of l_2 - 4 by 14.3% from 95.9% to 81.6%. The most heavily loaded tie-line is now shifted to l_2 - 11, which has 82.3% loading. Overall, the loading has become more uniformly distributed among all the tie-lines, as compared to that before the optimum topology is employed.

Case 4 is about the transitioning sequence effects. The above cases are based on STR and only the optimal topology is proposed. The transitioning sequence between the initial and optimal states and the effects of line rating (STR vs DTR) toward the transitioning sequence, which have not been investigated, are studied in this section. Case 2 is selected as the case study in this section. The best transitioning sequence to achieve its optimum topology, as shown in Table III, with the least

impact on the UPG, is investigated. Other cases can also be used and they would only affect the numerical values.

The DTR values considered here are based on the weather conditions at Haiyang, China at two different times: 1) hour 0000–0100 on 1/1/2019 (winter); and 2) hour 1100–1200 on 1/6/2019 (summer). The weather data of these two times, along with the calculated DTR values of the tie-lines 110-LGJ-95, are shown in Table IV. The STR of the conductor is 310 A, based on $V_\omega = 0.5$, $\theta_\omega = 0$, $T_a = 40$ and $T_c = 100$. For simplification, the capacity of the tie-lines between STs is not considered. It is also considered that the distribution lines are underground cables which have very different thermal behavior than the overhead lines. As the IEEE 738 standard is used to describe the DTR system, which is only suitable for overhead lines, the DTR system is not applied to the DNs (unit groups). As a result, the DTR system is only considered in the tie-lines between the STs and DN. STR and DTR are implemented by replacing $I_{\max,l}$ in (22) for all the tie-lines. Depending on the chosen line rating values, different optimum transitioning sequences are obtained and their impact is shown in Table V.

TABLE IV
WEATHER DATA AND DTR VALUES

No.	V_ω (m/s)	θ_ω (°)	T_a (°C)	T_c (°C)	DTR (A)
1	4.06	31.01	−5.1	100	507
2	1.86	30.34	15.9	100	342

TABLE V
VARIOUS TRANSITIONING SEQUENCES AND THEIR IMPACTS IN CASE 4

No.	$I_{\max}$ (A)	Transitioning sequence	$\sum_{R=1}^{10} f_U^R$	$\sum_{R=1}^{10} f_I^R$
1	310	l_2-9; 301–302; 301–303; 303–308; l_2-12; 201–202; 201–204; l_2-6; 104-113; l_2-3	4.67	5.37
2	342	l_2-12; 201-202; l_2-9; 301–302; 301–303; 303–308; 201–204; l_2-6; 104-113; l_2-3	4.86	4.90
3	507	l_2-9; 301–302; 301–303; 303–308; 201–204; 201–202; l_2-12; l_2-6; 104–113; l_2-3	4.67	3.30
4	507	301–303; 303–308; 104–113; l_2-3; 201–204; l_2-6; l_2–12; 201-202; l_2-9; 301–302	8.82	3.44

The first and second sequences are the optimum transitioning sequences based on STR (310 A) and DTR2 (342 A), respectively, whereas the third and fourth sequences are the optimum and worst transitioning sequences based on DTR1 (507 A).

The impact of the first transitioning sequence based on STR is worse than the second and third sequences. This is expected because STR limits power flows which creates more congestion than when DTR is employed. For example, line l_2-13 remains congested until line l_2-12 is closed, which enables some of its loading to be shared by l_2-12. Interestingly, the third transitioning sequence based on the highest DTR value, i.e., DTR1 (507 A), is about the same as the first sequence. The only difference is the switching sequence of the two lines, i.e., l_2-12 and 201–204, are opposite to each other. However, it is noted that the impact of line overloading in the third sequence is significantly lower than the first sequence, by 39%. Switching the line 201–204 before line l_2-12 causes tie-line l_2-6 to overload in the first sequence, but the same problem is avoided in the third sequence.

The second sequence employs a lower DTR value than the third sequence. In the second sequence, the lines in unit group A_2 have to be switched first in order to keep the loading of all lines under DTR2 (342 A). Consequently, the voltage levels in A_3 are compromised, and the total impact of the voltage deviation of the second sequence is higher than in the third sequence by 4.1%. The higher DTR1 used in the third sequence causes less overloading when transitioning through the line switching sequence, resulting in 32.6% lower total line overloading impact than the second sequence.

The third (optimum) and fourth (worst) sequences are based on the same DTR1 (507 A), and are used to demonstrate the effects of different transitioning sequences at the same DTR level. Both impact indicators of the fourth sequence are worse than the third sequence. The reason is that switching the lines 301–303 and 303–308 first in the fourth sequence increases the loading of tie-line l_2-14 to 102.37% of DTR1 (507 A). At the same time, all the nodal voltages from 301 to 307 and from 311 to 314 dip to around 0.82 p.u., which is below the allowable range (0.93–1.07 p.u.). This adverse situation lasts almost until the end of the sequence and is cleared only after the 9th line is switched, i.e., closing line l_2-9. In the third sequence, the highest line loading is only 349 A in l_2-13, which is lower than its DTR1 maximum capacity. Therefore, all the tie-lines are operating within the allowable limit. In addition, all nodal voltages of the third sequence are also within the allowable range during the entire transitioning sequence. Thus, the third sequence outperforms the fourth sequence on both impact indicators.

Case 5 is about performance benchmarking. considering that the biggest problem of flexible topology is the rate of finding solution, the abilities of ACOPF [3], PSOA (0-1 coding), and SOCP [3] are compared with the proposed method in mitigating congestion in this case. The ACOPF, PSOA (0-1 coding), and SOCP are solved by MIP, MATLAB, and CPLEX, respectively. The computing times, load shedding and safety margins of these methods are shown in Table VI. The definition of safety margin is shown as:

$$f = \max\left\{\frac{I}{I_{\max,l}}\right\} \tag{27}$$

where the margin is the maximum capacity after mitigating congestion. Smaller margin values indicate a safer operation, while the maximum capacity in this paper here is the STR.

In terms of computation time, the proposed method is significantly faster than the PSOA (0-1 coding) because the TSO and DSO are decoupled by the two-layer model. Although the proposed method is slower than the ACOPF, load shedding is avoided in the proposed method while present in the ACOPF. The SOCP performs equally well as the proposed method in terms of computation speed and load shedding, but the proposed method has a smaller safety margin. In fact, the safety margin of the proposed method is the lowest among all the methods shown in Table VI.

TABLE VI
VARIOUS TRANSITIONING SEQUENCES AND THEIR IMPACTS IN CASE 5

Methods	Time (s)	Load shedding (p.u.)	Safety margin
ACOPF [3]	0.37	0.105	0.79
PSOA (0-1 coding)	175.5	0.216	0.63
SOCP [3]	1.7	0	0.82
Proposed method	1.73	0	0.56

VII. CONCLUSION

This paper proposes a two-layer congestion mitigation framework of a UPG, while also considering the transitioning sequence between the initial and optimal states of the UPG. The results show that the proposed framework is able to mitigate UPG congestion with sporadic load growth (Case 1), large scale load growth (Case 2) and N-1 line outages (Case 3). The effects of STR and DTR on the transitioning sequence have also been demonstrated and compared. The layering approach in the proposed framework enables a faster computation and produces topologies with sufficient safety margin. Hence, this approach is well-suited for implementation in large-scale UPGs, harnessing the benefits of their flexible topologies, and achieving substantial power flow transfer and load balancing. It has significant value for engineering application.

AUTHORS' CONTRIBUTIONS

Yi Su: draft and revision writing. Jiashen Teh: supervision. Qian Luo, Kangmiao Tan, and Jiaying Yong: writing-review and editing. All authors read and approved the final manuscript.

FUNDING

This work is supported by the Universiti Sains Malaysia, Research University Team (RUTeam) Grant Scheme (No. 1001/PELECT/8580011).

AVAILABILITY OF DATA AND MATERIALS

Please contact the corresponding author for data material request.

DECLARATIONS

Competing interests: The authors declare that they have no known competing financial interests or personal relationships that could have appeared to influence the work reported in this article.

AUTHORS' INFORMATION

Yi Su received his B.S. degree in electrical engineering and automation from Wuhan University of Technology, Wuhan, China in 2009, his M.S. degree in electrical engineering from Hunan University, Changsha, China in 2016 and his Ph.D. degree in power systems and energy conversion from Universiti Sains Malaysia (USM) in 2024. Now he is the assistant professor at Xiangtan University, China. From 2016 to 2020, he was an engineer at China Southern Power Grid. His research interests include resilience of distribution networks, optimized control of power systems, and intelligent information processing.

Jiashen Teh received his B.Eng. degree (Hons.) in electrical and electronic engineering from Universiti Tenaga Nasional, Malaysia in 2010 and his Ph.D. degree in electrical and electronic engineering from The University of Manchester, Manchester, U.K. in 2016. Since 2023, he has been an assistant professor at Universiti Sains Malaysia (USM), Malaysia. He is a chartered engineer conferred by the Engineering Council, U.K. and the Institution of Engineering and Technology, as well as a registered professional engineer with the Board of Engineers Malaysia. His research interests include probabilistic modeling of power systems, grid integration of renewable energy sources, and reliability modeling of smart grid networks. For three consecutive years in 2019, 2020 and 2021, he was among the top 2% of the world's most cited researchers according to field ranked by Stanford University. In 2021, he was given the IEEE PES Malaysia Outstanding Engineer Award. (E-mail: jiashenteh@usm.my)

Qian Luo is with the School of Computer Sciences, Universiti Sains Malaysia (USM), 11800 Penang, Malaysia.

Kangmiao Tan is with the Institute of Power Engineering, College of Engineering, Universiti Tenaga Nasional (UNITEN), 43000 Kajang, Selangor, Malaysia.

Jiaying Yong is with the Institute of Power Engineering, College of Engineering, Universiti Tenaga Nasional (UNITEN), 43000 Kajang, Selangor, Malaysia.

REFERENCES

[1] Y. Che, J. Jia, and Y. Zhao *et al*., "Vulnerability assessment of urban power grid based on combination evaluation," *Safety Science*, vol. 113, pp.144-153, Mar. 2019.

[2] T. Kang, J. Zhu, and C. Feng *et al*., "An orderly charging strategy for a photovoltaic-storage-charging integrated community ." *Power System Protection and Control*, vol. 52, no. 9, pp:132-142, May. 2024.(in Chinese)

[3] X. Zhang, Y. Liu, and H. Gao *et al*., "A bi-level corrective line switching model for urban power grid congestion mitigation," *IEEE Transactions on Power Systems*, vol. 35, no. 4, pp. 2959-2970, Jul. 2020.

[4] K. Chakravarthi, P. Bhui, and N. K. Sharma *et al*., "Real time congestion management using generation re-dispatch: modeling and controller design," *IEEE Transactions on Power Systems*, vol. 38, no. 8, pp. 2189-2203, May 2023.

[5] J. Shi and S. S. Oren. "Stochastic unit commitment with topology control recourse for power systems with large-scale renewable integration," *IEEE Transactions on Power Systems*, vol. 33, no. 3, pp. 3315-3324, May 2017.

[6] M. H. Moradi, A. Reisi, and S. M. Hosseinian. "An optimal collaborative congestion management based on implementing DR," *IEEE Transactions on Smart Grid*, vol. 9, no. 5, pp. 5323-5334, Mar. 2017.

[7] F. Shen, Q. Wu, and S. Huang *et al*., "Two-tier demand response with flexible demand swap and transactive control for real-time congestion management in distribution networks," *International journal of electrical power and energy systems*, vol. 114, Jan. 2020.

[8] M. Mousavi and M. Wu. "A DSO framework for market participation of DER aggregators in unbalanced distribution networks," *IEEE Transactions on Power Systems*, vol. 37, no. 3, pp. 2247-2258, Oct. 2021.

[9] A. Kargarian and Y. Fu. "System of systems based security-constrained unit commitment incorporating active distribution grids," *IEEE Transactions on Power Systems*, vol, 29, no. 5, pp. 2489-2498, Mar. 2014.

[10] Y. Weng, J.Xie, and P. Wang *et al*., "Asymmetrically reciprocal effects and congestion management in TSO-DSO coordination through feasibility regularizer," *IEEE Transactions on Power Systems*, vol. 38, no. 2, pp. 1948-1962, Mar. 2023.

[11] A. Vicente-Pastor, J. Nieto-Martin, and D. W. Bunn *et al*., "Evaluation of flexibility markets for retailer-DSO-TSO coordination," *IEEE Transactions on Power Systems*, vol. 34, no. 3, pp. 2003-2012, May 2019.

[12] H. Chen, D. Wang, and R. Zhang *et al*., "Optimal participation of ADN in energy and reserve markets considering TSO-DSO interface and DERs uncertainties," *Applied Energy*, vol. 308, Feb. 2022.

[13] C. Lai and J. Teh. "Network topology optimisation based on dynamic thermal rating and battery storage systems for improved wind penetration and reliability," *Applied Energy*, vol. 305, Jan. 2022.

[4] Y. Gao, W. Wang, and J. Shi *et al*., "Batch-constrained reinforcement learning for dynamic distribution network reconfiguration," *IEEE Transactions on Smart Grid*, vol. 11, no. 6, pp. 5357-5369, Nov. 2020.

[15] R. Pegado, Z. Ñaupari, and Y. Molina *et al*., "Radial distribution network reconfiguration for power losses reduction based on improved selective BPSO," *Electric Power Systems Research*, vol. 169, pp. 206-213, Apr. 2019.

[16] Y. Wang and B. Yang, "Optimal PV array reconfiguration under partial shading condition through dynamic leader based collective intelligence," *Protection and Control of Modern Power Systems*, vol. 8, no. 3, pp. 1-16, Jul. 2023.

[17] H. Wu, P. Dong, and M. Liu, "Distribution network reconfiguration for loss reduction and voltage stability with random fuzzy uncertainties of renewable energy generation and load," *IEEE Transactions on Industrial Informatics*, vol. 16, no. 9, pp. 5655-5666, Sept. 2020.

[18] A. Arefi, G. Ledwich, and G. Nourbakhsh *et al*., "A fast adequacy analysis for radial distribution networks considering reconfiguration and DGs," *IEEE Transactions on Smart Grid*, vol. 11, no. 5, pp. 3896-3909, Sept. 2020.

[19] Y. Su and J. Teh. "Two-stage optimal dispatching of AC/DC hybrid active distribution systems considering network flexibility," *Journal of Modern Power Systems and Clean Energy*, vol. 11, no. 1, pp. 52-65, Jan. 2023.

[20] L. Zhang, J. Liang, and W. Tang e*t al*., "Converting AC distribution lines to DC to increase transfer capacities and DG penetration," *IEEE Transactions on Smart Grid*, vol. 10, no. 2, pp. 1477-1487, Mar. 2019.

[21] Code on security and stability for power system, GB/T 38755-2019, 2019. (in Chinese)

[22] Economical operation for power transformers, GB/T 13462-2008, 2008. (in Chinese)

[23] T. Barton and P. Musilek. "Probabilistic forecasting of dynamic thermal line rating with temporal correlations," *International Journal of Electrical Power and Energy Systems*, vol. 134, Jan. 2022.

[24] Y. Su, J. Teh, and C. Chen."Optimal dispatching for AC/DC hybrid distribution systems with electric vehicles: application of cloud-edge-device cooperation," *IEEE Transactions on Intelligent Transportation Systems*, vol. 25, no. 3, pp. 3128-3139, 2024.

[25] J. Chen, H. Chen, and Z. Liang *et al*., "An exergy analysis model for the optimal operation of integrated heat-and-electricity-based energy systems," *Protection and Control of Modern Power Systems*, vol. 9, no.1, pp. 1-18, Jan. 2024.

[26] Y. Xu and J. Zhang. "A two-layer two-stage dispatching strategy for active distribution network with micro-grid considering multiple interactions," *Electric Power Systems Research*, vol. 187, Oct. 2020.